SIMPLIFIED MODEL OF SEGMENTED
ELECTRODE LOSSES IN
NONEQUILIBRIUM MHD GENERATORS

Myron A. Hoffman
Space Propulsion Laboratory
Department of
Aeronautics and Astronautics

CSR TR-66-7   August 1966

SIMPLIFIED MODEL OF SEGMENTED ELECTRODE

LOSSES IN NONEQUILIBRIUM MHD GENERATORS

Myron A. Hoffman*

Abstract

Linear, segmented electrode MHD generators designed to utilize non-equilibrium ionization have not yet produced the expected performance. Kerrebrock[1,2] proposed that this could be due to shorting of the Hall current along the electrode wall. A simplified two-layer model of these important generator non-uniformities is proposed in this paper. Solutions of the resulting set of algebraic equations exhibit the same essential behavior as Kerrebrock's more complete theoretical formulation[2]. In particular, the equations yield the "normal" and the "shorted" modes found by Kerrebrock and permit the calculation of the stability boundary between these modes.

(1) Kerrebrock, J.L., "Segmented Electrode Losses in MHD Generators with Nonequilibrium Ionization - I" Avco RR 178, April 1964.

(2) Kerrebrock, J.L., "Segmented Electrode Losses in MHD Generators with Nonequilibrium Ionization - II" Avco RR 201, January 1965.

* Associate Professor of Aeronautics and Astronautics, Massachusetts Institute of Technology, Cambridge, Mass.

Acknowledgement

1. Simplified Model

In order to solve for the steady state behavior of an MHD generator with segmented electrodes, we will start with the following steady flow MHD equations without viscosity or heat conduction and with steady electric and magnetic fields:

Continuity:
$$\nabla \cdot (\rho \bar{u}) = 0 \qquad (1)$$

Momentum:
$$\rho (\bar{u} \cdot \nabla) \bar{u} = -\nabla p + \bar{J} \times \bar{B} \qquad (2)$$

Energy:
$$\rho (\bar{u} \cdot \nabla)\left(h + \frac{u^2}{2}\right) = \bar{J} \cdot \bar{E} \qquad (3)$$

Eq. of State:
$$p = \rho R T \qquad (4)$$

Maxwell's Eqs:
$$\nabla \cdot \bar{E} = \frac{\rho_c}{\epsilon_0} \qquad (5)$$

$$\nabla \cdot \bar{B} = 0 \qquad (6)$$

$$\nabla \times \bar{E} = 0 \qquad (7)$$

$$\nabla \times \bar{B} = \mu_0 \bar{J} \qquad (8)$$

Current Conservation:
$$\nabla \cdot \bar{J} = 0 \qquad (8')$$

Ohm's Law:
$$\bar{J} = \sigma \bar{E}' - \frac{\beta}{B} \bar{J} \times \bar{B} \qquad (9)$$

Electron Energy Balance:
$$\bar{J} \cdot \bar{E}' = \frac{\delta m_e}{m_a} \nu_e n_e \frac{3}{2} k (T_e - T_a) \qquad (10)$$

Saha Eq:
$$\frac{n_e^2}{n_{so} - n_e} = \left(\frac{2\pi m_e k T_e}{h^2}\right)^{\frac{3}{2}} e^{-\frac{e\phi_i}{kT_e}} \qquad (11)$$

Conductivity: $$\sigma = \frac{e^2 n_e}{m_e \nu_e}$$ (12)

where an effective energy loss parameter, δ ; the average heavy species mass, m_a ; and the total electron collision frequency should be used for a mixture of gases.

In order to solve this formidable array of equations, we make the following simplifying assumptions (following Kerrebrock[1,2]). First, we assume that the interaction length, L*, is large compared to the electrode spacing, 2L. For slowly varying duct area, the free-stream fluid velocity and thermodynamic properties can then be assumed to be constant over a few electrode spacings. Second, we ignore viscous effects in the electrode wall layer. These assumptions essentially decouple the fluid mechanics from the electrical effects. That is, Eqs. (5-12) can now be solved independently of Eqs. (1-4), using average fluid properties.

The plasma approximation, which was already implicit in Eqs. (2) and (8), decouples Eq. (5) from the remaining equations. Similarly, the assumption of small magnetic Reynolds number decouples Eq. (8), and for a uniform magnetic field in the z direction, Eq. (6) yields no new information.

These assumptions leave us with the task of solving Eqs. (7-12) with appropriate boundary conditions and with some model of the electrode wall layer. In the simplified model of this paper, the assumption is made that we can use average

values of the electron and gas temperatures, designated T_{ew} and T_w, to characterize the electrode wall layer (EWL). In addition, average values for all other important variables in each of the two regions are employed. This approach is not unlike that taken by Rosa[3] to evaluate the effect of various generalized non-uniformities on MHD generator performance.

It should be noted that the above simplified model assumes complete uniformity in the B field direction. As a result all effects due to the insulator wall boundary layers have been ignored.

These assumptions reduce the original two differential and four algebraic equations to the following set of fourteen algebraic equations for the two regions defined in Fig. 1:

$$V_y = -2 \left(E_{yw} \lambda + E_{y\infty} H \right) \tag{13}$$

$$E_{xw} = C_E E_{x\infty} \tag{14}$$

$$j_{xw} = -C_x j_{x\infty} \tag{15}$$

$$j_{yw} = C_y j_{y\infty} \tag{16}$$

$$E_{x\infty} = \frac{j_{x\infty}}{\sigma_\infty} + \frac{\beta_\infty}{\sigma_\infty} j_{y\infty} \tag{17}$$

$$E_{xw} = \frac{j_{xw}}{\sigma_w} + \frac{\beta_w}{\sigma_w} j_{yw} \tag{18}$$

$$E_{y\infty} - u_\infty B = \frac{j_{y\infty}}{\sigma_\infty} - \frac{\beta_\infty}{\sigma_\infty} j_{x\infty} \tag{19}$$

$$E_{yw} - u_w B = \frac{\dot{j}_{yw}}{\sigma_w} - \frac{\beta_w}{\sigma_w} \dot{j}_{xw} \qquad (20)$$

$$\frac{\dot{j}_\infty^2}{\sigma_\infty} = \delta_\infty \frac{m_e}{m_a} n_{e\infty} \nu_{e\infty} \frac{3}{2} k \left(T_{e\infty} - T_\infty\right) \qquad (21)$$

$$\frac{\dot{j}_w^2}{\sigma_w} = \delta_w \frac{m_e}{m_a} n_{ew} \nu_{ew} \frac{3}{2} k \left(T_{ew} - T_w\right) \qquad (22)$$

$$n_{e\infty} \cong \left(\frac{2\pi m_e k T_{e\infty}}{h^2}\right)^{\frac{3}{4}} e^{-\frac{e\phi_i}{2 k T_{e\infty}}} \qquad (23)$$

$$n_{ew} \cong \left(\frac{2\pi m_e k T_{ew}}{h^2}\right)^{\frac{3}{4}} e^{-\frac{e\phi_i}{2 k T_{ew}}} \qquad (24)$$

$$\sigma_\infty = \frac{e^2 n_{e\infty}}{m_e \nu_{e\infty}} \qquad (25)$$

$$\sigma_w = \frac{e^2 n_{ew}}{m_e \nu_{ew}} \qquad (26)$$

The parameter, C_E, is a measure of the way in which E_{xw} increases above the insulator segment in the EWL. As a first approximation, simple geometrical arguments lead to:

$$C_E \sim \frac{L}{L-\ell}$$

Similarly, C_x measures the concentration of the Hall current in the EWL. Once again simple geometrical arguments lead to the conclusion that $C_x \sim H/h$. As a rough first approximation, h can be taken to be of order L.

The parameter, C_y, is a measure of the way in which j_y concentrates or increases as the current flows from the freestream through the electrode wall layer. It is related

to L/ℓ but it will very likely vary significantly for different operating conditions. It should be noted that the simplified model of this paper introduces this additional empirical parameter which is not required in Kerrebrock's model.

The boundary conditions are, in effect, already built into these equations. In particular, the boundary conditions used by Kerrebrock[2] that $J_y = 0$ on the insulator segments and J_y = constant on the electrode segments are both contained implicitly in C_y and C_x. This must be the case since the present model does not explicitly account for the variations in the x direction due to the electrode and insulator segments.

The equations can be put into a convenient non-dimensional form for the case of a segmented Faraday generator by introducing the following reference current density, reference electron temperature rise, and reference voltages:

$$j_{ref} \triangleq -\sigma_\infty \left[u_\infty B + \frac{V_t}{2(H+\hbar)} \right] = -\sigma_\infty u_\infty B (1-K) \tag{27}$$

$$\left(\frac{T_e}{T_\infty}-1\right)_{ref} \triangleq \frac{j_{ref}^2}{\sigma_\infty} \frac{1}{\delta_e \frac{m_e}{m_a} n_{e\infty} \nu_{e\infty} \frac{3}{2} k T_\infty}$$

$$= \frac{2\gamma}{3\delta_e} M_\infty^2 \beta_\infty^2 (1-K)^2 \tag{28}$$

where δ_e = the ideal elastic energy loss parameter.

$$V_{x(ref)} \triangleq - \frac{2L\, j_{ref}\, \beta_\infty}{\sigma_\infty} \qquad (29)$$

$$V_{yw(ref)} \triangleq V_y \left(\frac{h}{2H+2h} \right) \qquad (30)$$

The reference voltage of Eq. (30) is that transverse voltage drop across the EWL which would exist if the transverse electric field were completely uniform across the channel.

The final set of non-dimensional equations can be written as follows:

$$\frac{j_{x\infty}}{j_{y\infty}} = \frac{-\beta_\infty \left(1 - \frac{C_y}{C_E} N \right)}{\left(1 + \frac{C_x}{C_E} \frac{N}{G} \right)} \qquad (31)$$

$$\frac{j_{y\infty}}{j_{ref}} = \frac{1 + \frac{h}{H} \left(1 - \frac{1-U}{1-K} \right)}{\left(1 + \frac{N}{G} \frac{h}{H} C_y \right) + \beta_\infty \left(\frac{j_{x\infty}}{j_{y\infty}} \right) \left(C_x \frac{h}{H} N - 1 \right)} \qquad (32)$$

$$\left(\frac{j_\infty}{j_{ref}} \right)^2 = \left(\frac{j_{y\infty}}{j_{ref}} \right)^2 \left[1 + \left(\frac{j_{x\infty}}{j_{y\infty}} \right)^2 \right] \qquad (33)$$

$$\left(\frac{j_w}{j_{ref}} \right)^2 = \left(\frac{j_{y\infty}}{j_{ref}} \right)^2 \left[C_y^2 + C_x^2 \left(\frac{j_{x\infty}}{j_{y\infty}} \right)^2 \right] \qquad (34)$$

$$\tau_\infty \triangleq \frac{\left(\frac{T_{e\infty}}{T_\infty} - 1 \right)}{\left(\frac{T_e}{T_\infty} - 1 \right)_{ref}} = \left(\frac{j_\infty}{j_{ref}} \right)^2 \frac{\delta_e}{\delta_\infty} \qquad (35)$$

$$\tau_w \triangleq \frac{\left(\frac{T_{ew}}{T_w} - 1\right)}{\left(\frac{T_e}{T_\infty} - 1\right)_{ref}} = \left(\frac{j_w}{j_{ref}}\right)^2 \frac{\delta_e}{\delta_w} \frac{N^2}{G} \tag{36}$$

$$\left(\frac{T_e}{T_\infty} - 1\right)^2_{ref} + \left[\frac{\lambda_w}{G \ln N}\left(\frac{G}{\tau_\infty} - \frac{1}{\tau_w}\right) + \left(\frac{1}{\tau_\infty} + \frac{1}{\tau_w}\right)\right] \times \tag{37}$$

$$\left(\frac{T_e}{T_\infty} - 1\right)_{ref} + \frac{1}{\tau_\infty \tau_w}\left[1 + \frac{(G-1)\lambda_\infty}{G \ln N}\right] = 0$$

$$\frac{V_{xw}}{V_{x(ref)}} = \left(\frac{j_{y\infty}}{j_{ref}}\right)\left[\frac{C_y}{C_E} N - \frac{C_x N}{C_E G} \frac{1}{\beta_\infty}\left(\frac{j_{x\infty}}{j_{y\infty}}\right)\right] \tag{38}$$

$$\frac{V_{yw}}{V_{yw(ref)}} = -\left(\frac{j_{y\infty}}{j_{ref}}\right)\left[\frac{C_y N}{G} + C_x N \beta_\infty\left(\frac{j_{x\infty}}{j_{y\infty}}\right)\right]\left(\frac{1-K}{K}\right) + \frac{U}{K} \tag{39}$$

In these equations we have introduced the following additional non-dimensional variables:

$$N \triangleq \frac{n_{e\infty}}{n_{ew}} \tag{40}$$

$$G \triangleq \frac{T_w}{T_\infty} \tag{41}$$

$$U \triangleq \frac{\mu_w}{\mu_\infty} \tag{42}$$

In the above equations the Hall parameter ratio and collision frequency ratio have been approximated by:

$$\frac{\beta_w}{\beta_\infty} = \frac{\nu_{e\infty}}{\nu_{ew}} \approx G \tag{43}$$

The electrical conductivity approximation used is for a slightly ionized gas where electron-neutral atom collisions dominate:

$$\frac{\sigma_\infty}{\sigma_w} \approx \frac{N}{G} \tag{44}$$

These approximations assume that $\sqrt{T_{ew}/T_{e\infty}}$ is close to unity and that coulomb collisions can be neglected. In addition, an approximate form of the Saha Eq. has been used to relate the electron density to the electron temperature:

$$\frac{n_{ew}}{n_{e\infty}} \approx e^{-\lambda_\infty \frac{T_\infty}{T_{e\infty}} \left(\frac{T_{e\infty}}{T_{ew}} - 1\right)} \tag{45}$$

where

$$\lambda_\infty \triangleq \frac{e\phi_i}{2kT_\infty}$$

Furthermore, the following sort of averages are implicit in this model:

$$\langle j_{yw}^2 \rangle \approx \langle j_{yw} \rangle^2 = \langle C_y j_{y\infty} \rangle^2 \tag{46}$$

and

$$\langle j_{xw}^2 \rangle \approx \langle j_{xw} \rangle^2 = \langle C_x j_{x\infty} \rangle^2 \tag{47}$$

These are clearly very rough approximations.

As can be seen from the above equations, the use of the actual free-stream σ_∞ , $n_{e\infty}$ and $\nu_{e\infty}$ in defining the reference conditions leads to very simple non-dimensional results. However, it should be pointed out that this reference case does not correspond to an ideal, infinitely-

segmented Faraday generator. For a given set of specified
values for M_∞, β_∞, K and δ_e the ideal values of σ,
n_e and ν_e corresponding to an infinitely segmented
generator would all be higher than the σ_∞, $n_{e\infty}$ and $\nu_{e\infty}$
used above. However, the free-stream Joule dissipation
would be the same for both the reference conditions and an
ideal, infinitely-segmented generator. That is:

$$\left(\frac{T_e}{T_\infty} - 1\right)_{ref} = \left(\frac{T_e}{T_\infty} - 1\right)_{inf} = \frac{2\gamma}{3\delta_e} M_\infty^2 \beta_\infty^2 (1-K)^2$$

As a result, it can easily be shown that the differences
between our selected reference conditions and those for an
ideal, infinitely-segmented generator do not affect the
calculated results for τ_∞. That is, the $\tau_\infty's$ obtained
non-dimensionalizing with either of the above cases are
identical. This makes the interpretation of the electron
temperature results quite straightforward.

This set of nine algebraic equations can be solved for
the complete performance of the generator if we specify
$\left(\frac{T_e}{T_\infty} - 1\right)_{ref}$, β_∞, U, G, λ_∞, δ_∞/δ_e, δ_w/δ_e, C_E, C_x and C_y.
In practice, it is more convenient to specify N and solve for
$\left(\frac{T_e}{T_\infty} - 1\right)_{ref}$. If we specify a given generator geometry,
working fluid and set of operating conditions, we can calcu-
late the first five parameters directly. In addition, δ_∞
and δ_w can be estimated assuming the major inelastic loss

is radiation using the approach taken by Kerrebrock in Ref. 4. This leads to the following relation for $\mathcal{S}_\infty$:

$$\frac{\mathcal{S}_\infty}{\mathcal{S}_e} = 1 + \frac{Q_\infty}{\mathcal{S}_e \frac{m_e}{m_a} n_{e\infty} \nu_{e\infty} \frac{3}{2} k T_\infty \left(\frac{T_{e\infty}}{T_\infty} - 1\right)} \tag{48}$$

where

$$Q_\infty \cong \left(\frac{2\pi e^2 n_o h \nu_o^3}{m_e c^3 \epsilon_o g_o}\right) e^{-\frac{h\nu_o}{k T_{e\infty}}} \sum_j 1.15 \left(\frac{2 g_o \gamma_{pj} \nu_j^2}{c^2 n_o g_j \gamma_{nj} D}\right)^{\frac{1}{2}} g_j f_{j\to o} \tag{49}$$

Assuming that the ionizable species is an alkali metal, we would sum over the two resonance lines (j = 1,2). Then n_0 is the density of alkali atoms in the ground state, ν_0 is the average frequency of the doublet for the alkali metals, γ_{nj} and γ_{pj} are the natural and pressure broadened line widths, g_0 and g_j are the degeneracies of the ground state and each first excited state, $f_{j\to o}$ is the oscillator strength for each resonance line, and D is the effective thickness of the free-stream plasma for radiation loss calculations. We approximate the ratio of the radiation loss from the EWL to the radiation loss from the free-stream by:

$$\frac{Q_w}{Q_\infty} \cong \left(\frac{D}{d}\right)^{\frac{1}{2}} N^{-\Lambda} \tag{50}$$

where $\Lambda \triangleq \dfrac{2 h \nu_o}{e \phi_i}$

and where d is the effective thickness of the EWL for radiation loss calculations. As a first approximation we can assume that $\left(\frac{D}{d}\right) \sim \left(\frac{H}{\lambda}\right)$ if the channel width in the B field direction is not too much less than the channel height. This Eq. (50) permits us to evaluate δ_w and eliminate it from Eq. (36) yielding:

$$\tau_w \cong \left(\frac{j_w}{j_{ref}}\right)^2 \frac{N^2}{G} - \tau_\infty \left(\frac{\delta_\infty}{\delta_e} - 1\right)\left(\frac{H}{\lambda}\right)^{\frac{1}{2}} N^{1-\Lambda} \tag{51}$$

In practice it is simpler to specify a series of representative values for β_∞ in solving Eqs. (31) to (39) and (51). Then Eq. (48) can be used to substantiate that the β_∞ is consistent with the $T_{e\infty}$'s in the region of interest.

It may also be necessary to refine the above estimate of δ_w to include the electronic heat conduction loss to the walls (see e.g. Lutz, Ref. 5).

This leaves C_E, C_x and C_y as semi-empirical parameters which can be adjusted to give agreement with experimental results. We can use the previous geometrical arguments to obtain a first approximation for these parameters.

2. Nature of Results

This simplified model of Kerrebrock's theory yields results with the same general features and characteristics as described in Ref. 2. In particular, the two-mode behavior sketched in Fig. 2 is obtained, the "normal" mode corresponding to values of $N>1$ and the "shorted" mode to values of $N<1$.

An examination of the equations reveals a great deal about the general nature of the phenomena involved. For example, Eq. (31) indicates the possibility of a sign change for $j_{x\infty}$ at a value of $N = \frac{c_E}{c_y}$. It should be noted that from geometrical arguments $\frac{c_E}{c_y} \sim \frac{l}{L-l}$ near $N\sim1$. This ratio will be of order unity for equal electrode and insulator segments.

For $N\frac{c_y}{c_E}<1$, the electrode wall layer (EWL) is more highly conducting than the free-stream resulting in large current flows above the insulator segments in the upstream direction. In the poorly conducting free stream, the current tries to flow along the lowest resistance path; i.e., at the Hall angle, (Fig. 3a).

For $N\frac{c_y}{c_E}>1$, the situation is probably reversed. That is, since the EWL is now of lower electrical conductivity, the current near the wall must try to flow at the Hall angle, (Fig. 3b).

The two-layer model representations of the x components of current for these two situations are shown in Figs. 3c and 3d. It can be seen that this simple interpretation of the current patterns can explain the x current reversals.

A similar examination of Eq. (39) reveals that V_{yw}, the voltage drop across the EWL, also experiences a sign reversal. The exact value of N where this sign reversal takes place is a rather complicated function of many parameters. However, it is easily seen from Eq. (39) that the sign is negative for $N \gg 1$ and positive for $N \ll 1$. This is physically reasonable since we would expect the voltage drop in the EWL to decrease as the EWL electrical conductivity increases (i.e. as N decreases). As a further check, it can be shown that Eq. (39) predicts that E_y becomes completely uniform for $N \sim 1$.

The limiting case of a uniform, continuous electrode generator can be obtained by causing the EWL to vanish. This requires setting $C_x = -1$, $C_y = +1$, $C_E = +1$, $\frac{h}{H} = 0$ and $N = G = U = 1$.

Then

$$\left(\frac{j_{x\infty}}{j_{y\infty}}\right) \Rightarrow -\beta_\infty$$

$$\left(\frac{j_{y\infty}}{j_{ref}}\right) \Rightarrow \frac{1}{1 + \beta_\infty^2}$$

It should be noted that for this limiting case C_x is no

longer simply related to $\frac{H}{h}$ as it is for the segmented electrode geometry.

For the segmented electrode generator in the shorted mode, the simplified two-layer model (Eqs. 31 and 32) predicts that $j_{y\infty}$ will vary approximately as follows $(N \ll 1)$:

$$\left(\frac{j_{y\infty}}{j_{ref}}\right)_{shorted} \sim \frac{1}{1 + \dfrac{\beta_{\infty}^2}{\left(1 + \dfrac{C_x N}{C_E G}\right)}}$$

This illustrates that for non-zero $C_x N / C_E G$ the segmented generator is not as severely shorted as a continuous electrode generator.

For the segmented electrode generator in the normal mode, the simplified two-layer model predicts that $j_{x\infty} / j_{y\infty}$ will be much less than unity for N not too much greater than unity and $C_x N / C_E G > \beta_{\infty}^2$. For this case we obtain the following approximate expressions valid for N near unity:

$$\left(and \ \frac{N}{G} \frac{h}{H} C_y \ll 1\right)$$

$$\left(\frac{j_{y\infty}}{j_{ref}}\right)_{normal} \sim 1 - \frac{N}{G} \frac{h}{H} C_y$$

$$\tau_{\infty(normal)} \sim \frac{\delta_e}{\delta_{\infty}} \left(1 - 2 \frac{N}{G} \frac{h}{H} C_y\right)$$

$$\left(\frac{V_{xw}}{V_{x(ref)}}\right)_{normal} \sim \frac{C_y N}{C_E}\left(1 - \frac{N}{G}\frac{\ell}{H}C_y\right)$$

$$\left(\frac{V_{yw}}{V_{yw(ref)}}\right)_{normal} \sim 1 + \left(\frac{1-K}{K}\right)\left[1 - \frac{C_y N}{G}\left(1 - \frac{N}{G}\frac{\ell}{H}C_y\right)\right]$$

These results are essentially the asymptotic behavior or the upper limit to the performance we can expect in the normal mode as $N \rightarrow 1$. It remains to determine where the stability boundary comes in to limit the performance attainable in the normal mode.

3. Stability Boundary

The typical performance behavior of this theory, shown in Fig. 2, possesses the "normal" mode and "shorted" mode characteristics discovered by Kerrebrock[2]. It is anticipated that the generator will operate in the mode of lowest total dissipation. Thus, the generator should make the transition to the lower curve (i.e. to the shorted mode) shown by the dashed line as the reference electron temperature is increased (i.e. as K is decreased for a given M_∞ and β_∞).

The "nose" of the shorted mode characteristic can be seen to define the probable stability boundary. It is possible to calculate the location of this stability boundary from Eq. (37) by setting $d\tau_\infty / d\left(\frac{T_e}{T_\infty} - 1\right)_{ref} = \frac{1}{0}$. This leads to the following stability requirement for operation in the normal mode:

$$\left(\frac{T_e}{T_\infty} - 1\right)_{ref}^* \tau_\infty^* \leq \frac{2(1-G)}{G^2 \beta_\infty^{*2}} \left(\frac{\delta_w}{\delta_\infty}\right)^* \tag{52}$$

where * represents the conditions at the nose of the shorted mode curve.

Substituting for $\left(\frac{T_e}{T_\infty} - 1\right)_{ref}$ from Eq. (28) we obtain:

$$M_\infty^{*2} \beta_\infty^{*4} \leq \frac{3\delta_e (1-G)}{\gamma G^2 (1-K^*)^2 \tau_\infty^*} \left(\frac{\delta_w}{\delta_\infty}\right)^* \tag{53}$$

Assuming that $\left(\delta_w/\delta_\infty\right)^*$ and τ_∞^* do not vary appreciably for different values of M_∞^* and β_∞^* we can draw some important conclusions from Eq. (53).

Since the maximum non-equilibrium electron temperature elevation is at the transition value of $\left(\frac{T_e}{T_\infty}-1\right)^*_{ref}$ it is proportional to $M_\infty^{*2}\,\beta_\infty^{*2}$. Therefore, it is highly desirable to operate at supersonic Mach numbers in order to obtain a high $T_{e\infty}$ at a low β_∞.

Furthermore, it can be seen from Eq. (53) that the stability boundary is very sensitive to the wall temperature through $\left(1-G/G^2\right)$. In fact, this two-layer model predicts that no electron temperature elevation is possible unless the wall is cooled below the static free stream gas temperature. This is probably not correct quantitatively, but does indicate the importance of a low electrode wall temperature in suppressing the EWL shorting. (Clearly the electrode thermionic emission requirements are in conflict with the cold wall requirement.)

By ignoring small terms in certain of the equations, an approximate solution for the conditions at the nose of the shorted-mode curve is possible. This leads to the following results:

$$\tau_\infty^* \sim \frac{1}{\left(\frac{\delta_\infty}{\delta_e}\right)^*\left[1+\frac{\beta_\infty^{*2}\left(1-NC_x\frac{A}{H}\right)^*\left(1-\frac{C_y}{C_E}N\right)^*}{\left(\frac{C_x N}{C_E G}\right)^*}\right]^2} \tag{54}$$

where
$$N^* \sim \left(\frac{C_E}{C_y}\right)^* \left[1 - \frac{1}{C_E^* \sqrt{2}}\right] \tag{55}$$

Putting this approximation into Eq. (52), we obtain an estimate of the value of $\left(\frac{T_e}{T_\infty} - 1\right)^*_{ref}$. Assuming that the maximum value of $T_{e\infty}$ occurs at this value of $\left(\frac{T_e}{T_\infty} - 1\right)^*_{ref}$ we can estimate the maximum value of the free-stream electron temperature rise in the normal mode.

$$\left(\frac{T_{e\infty}}{T_\infty} - 1\right)_{max} \sim \left(\frac{\delta_w}{\delta_\infty}\right)^* \frac{2(1-G)}{G^2 \beta_\infty^{*2}} \left[1 + \frac{\beta_\infty^{*2} \left(1 - N C_x \frac{R}{H}\right)^* \left(1 - \frac{C_y}{C_E} N\right)^*}{\left(\frac{C_x N}{C_E G}\right)^*}\right]^2 \tag{56}$$

In this approximation it has been assumed that τ_∞ in the normal mode at the stability boundary is of the order of $\left(\delta_e / \delta_\infty\right)$.

While numerical results using Eqs. (54) to (56) are not expected to be very accurate, the functional dependencies on the key parameters should be much more nearly correct. In particular, we can now examine the effect of generator size, electrode segmentation fineness, electrode wall temperature and Hall parameter on the maximum attainable electron temperature rise.

The parameter which is most closely related to the generator size is δ_∞ , since the radiation loss accounted for by this parameter is proportional to $H^{-\frac{1}{2}}$. All other things being equal, we see from Eq. (56) that $T_{e\infty(max)}$

should increase rather slowly with generator size. Further-more, from Eq. (52) we see that the value of $\left(\frac{T_e}{T_\infty}-1\right)^*_{ref}$ is almost independent of S_∞ and hence of generator size. These observations are in qualitative agreement with Kerre-brock's Fig. 13 in Ref. 2.

The segmentation fineness ratio is measured by (H/L) . If the EWL thickness, h, is assumed to be of order L, and further if we assume

$$C_x^* \sim \frac{H}{h} \sim \frac{H}{L}$$

then from Eq. (55) we can see that the maximum $T_{e\infty}$ tends to decrease as the segmentation fineness increases. This same trend was obtained by Kerrebrock[2] up to fairly high fineness ratios. Therefore, rather coarse segmentation ratios appear to be best, but the exact value to be used can not be specified from this model.

As the electrode wall temperature is decreased, the maximum attainable electron temperature rise increases very rapidly at first and then more slowly due primarily to the term $(1-G)/G^2$. For example, for a decrease in G from .90 to .45, increases in $\left(\frac{T_{e\infty}}{T_\infty}-1\right)_{max}$ of over a factor of twenty are predicted. This is in agreement with Kerrebrock's results in Fig. 7[2].

The dependence of the attainable electron temperature rise

on the free-stream Hall parameter, β_∞ , is somewhat more complicated:

$$\left(\frac{T_{e\infty}}{T_\infty} - 1\right)_{max} \sim \frac{1}{\beta_\infty^{*2}}\left[1 + F\,\beta_\infty^{*2}\right]$$

For the cases where F is much less than unity, namely for fine segmentation where C_x is large, the electron temperature rise is roughly proportional to β_∞^{-2} . This trend is, also, in agreement with Kerrebrock's Fig. 7[2].

4. Conclusions

The simplified two-layer model of Kerrebrock's segmented electrode loss theory appears to exhibit the essential behavior of the more complete theoretical formulation of Ref. 2. While the simple model does introduce one additional empirical parameter, it results in a set of simple, algebraic equations which can be easily interpreted and can be readily solved numerically once the empirical parameters are specified. In addition, it yields the important stability boundary between the normal and shorted modes.

REFERENCES

1. Kerrebrock, J.L., "Segmented Electrode Losses in MHD Generators with Nonequilibrium Ionization - I" Avco RR 178, April 1964.

2. Kerrebrock, J.L., "Segmented Electrode Losses in MHD Generators with Nonequilibrium Ionization - II" Avco RR 201, January 1965.

3. Rosa, R.J., "The Hall and Ion Slip Effects in a Non-uniform Gas" Avco RR 121, December 1961.

4. Kerrebrock, J.L., "Magnetohydrodynamic Generators with Nonequilibrium Ionization," AIAA Journal, Vol. 3, No. 4, April 1965.

5. Lutz, M.A., "Radiation and Its Effect on the Nonequilibrium Properties of a Seeded Plasma," Ph.D. Thesis, M.I.T. Dept. of Aeronautics and Astronautics, September 1965.
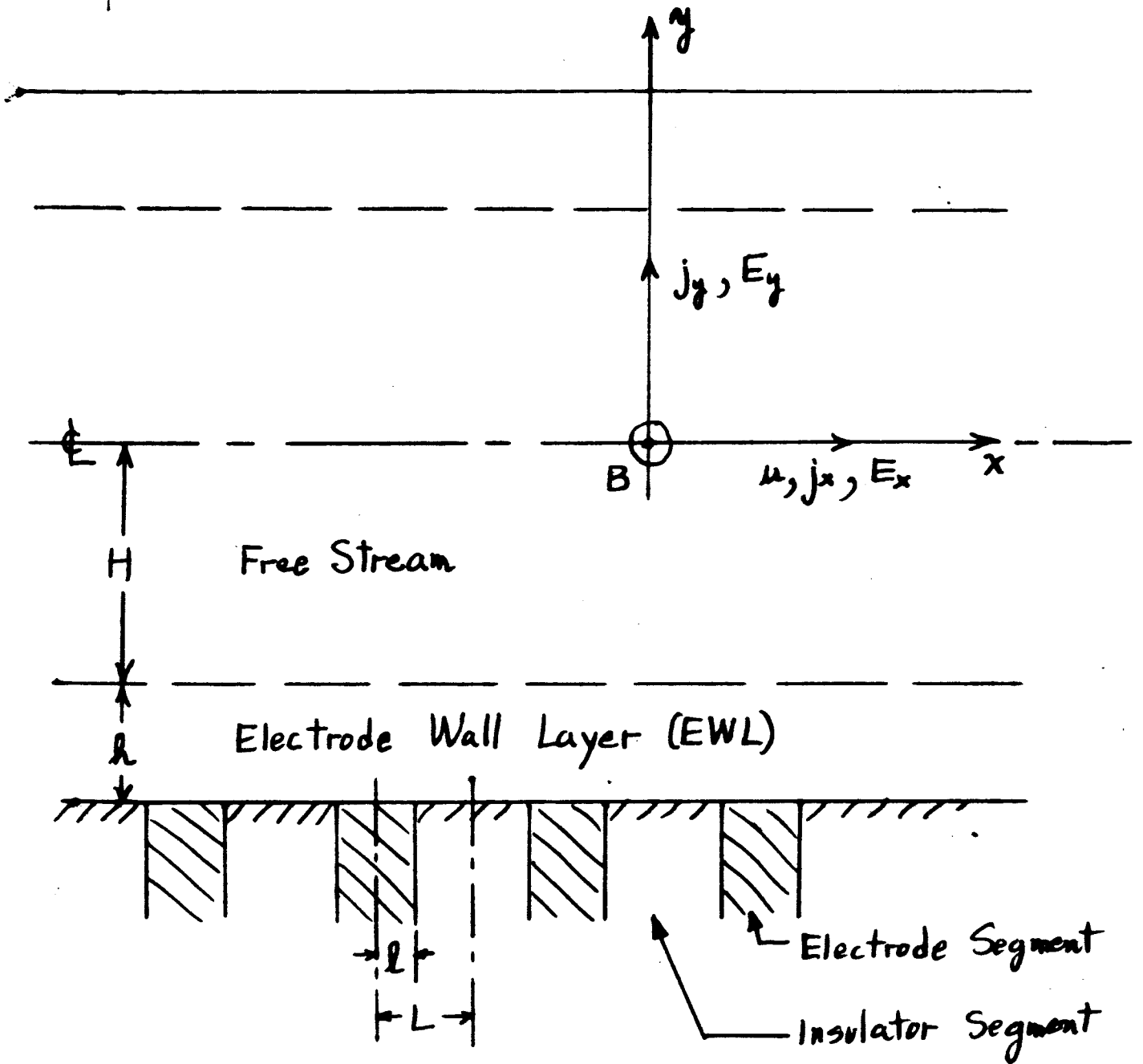
Fig. 1. Sketch of "two-layer" model of generator including definitions of regions, coordinate system and sign conventions used.

$$\tau_\infty \triangleq \frac{\left(\frac{T_{e\infty}}{T_\infty} - 1\right)}{\left(\frac{T_e}{T_\infty} - 1\right)_{ref}}$$

$\beta_\infty,\ G,\ U,\ \dfrac{\delta_\infty}{\delta_e}$, and geometry all fixed
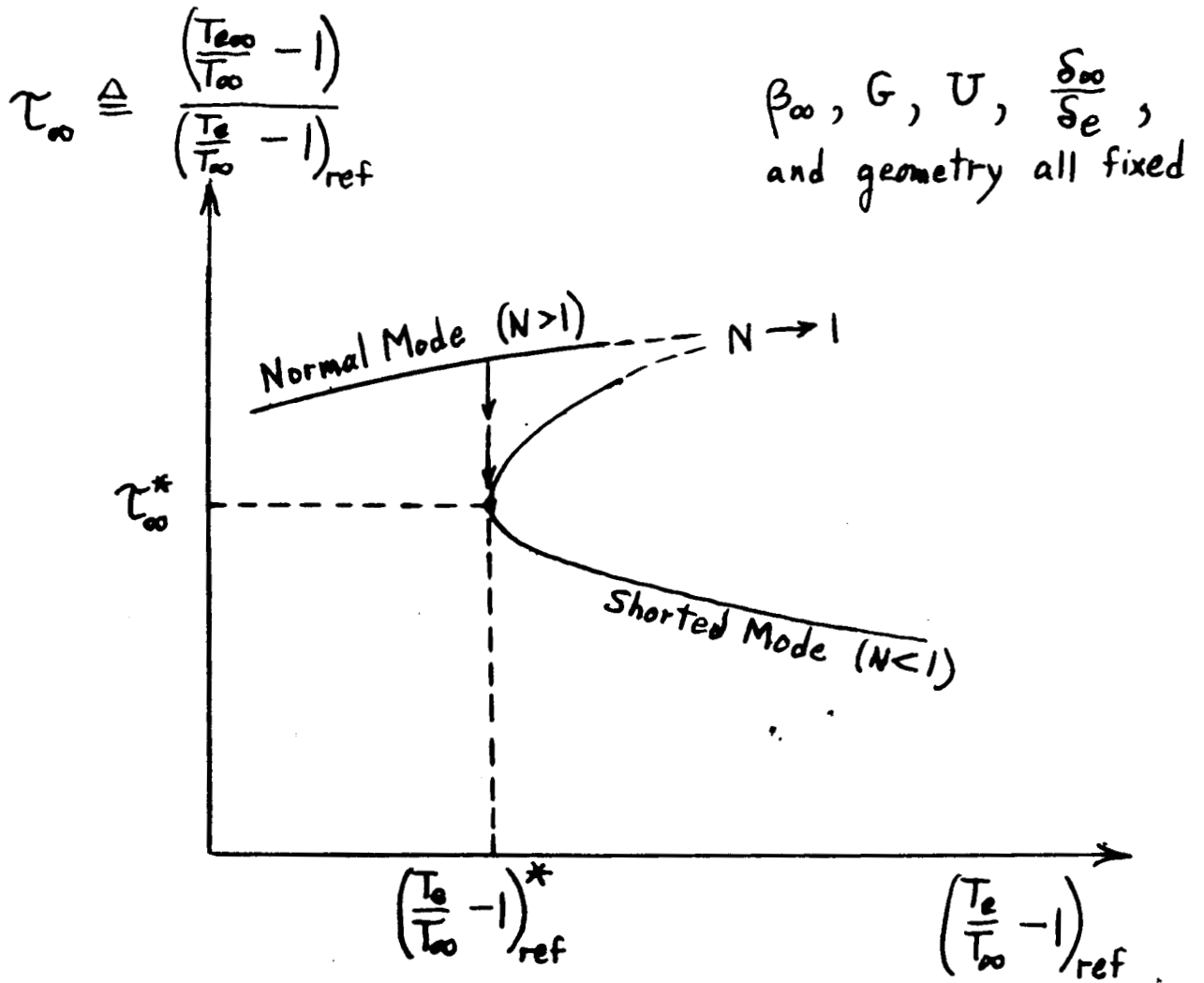

Fig. 2. Typical results for the electron temperature rise
for a specified geometry showing the probably
transition between modes at the nose of the shorted
mode characteristic.

3

Shorted Mode
$(N \ll 1)$

(a.)

Normal Mode
$(N \gg 1)$

(b.)

(c.)

(d.)

Anode

Cathode
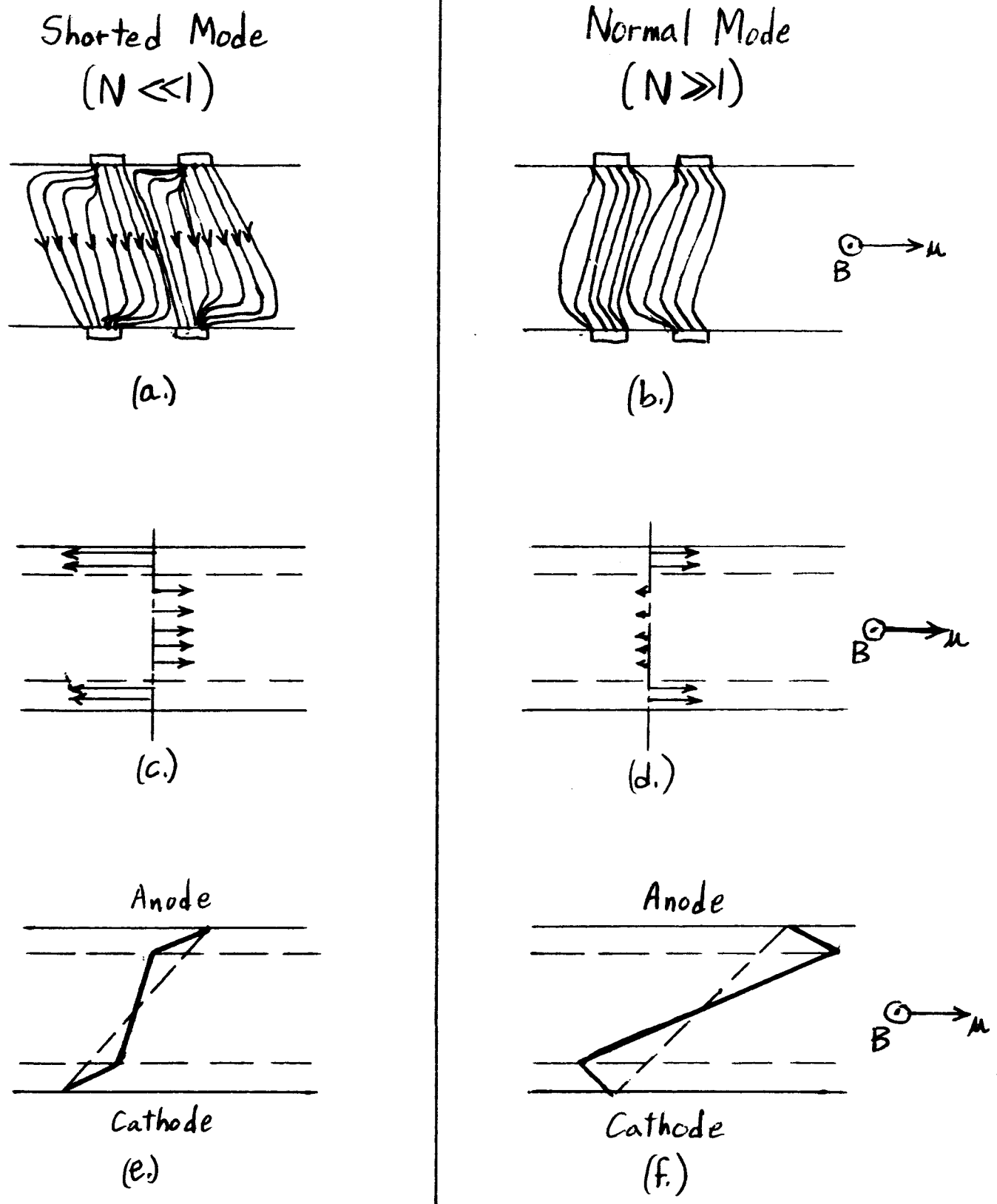
(e.)

Anode

Cathode

(f.)

Fig. 3.   Sketch of a possible set of current patterns for
the two modes in (a) and (b). The corresponding
x components of current in (c) and (d), and the
transverse voltage distributions in (e) and (f)
are those predicted by simplified two-layer model.